

Available online at website: https://journal.bcrec.id/index.php/bcrec

Bulletin of Chemical Reaction Engineering & Catalysis, 19 (4) 2024, 635-648



Research Article

Sonochemically Modified Lapindo Mud Using Sulfuric Acid for Efficient Adsorption of Phenol in Aqueous Media and Real Wastewater Samples

Karna Wijaya¹, Adyatma Bhagaskara¹, Maria Francia Mirabella Sani¹, Marini Fairuz Vebryana¹, Fernando Alvaro Pratama¹, Widuri Anggraeni¹, Amalia Kurnia Amin², Faturrahman Al Ramadhani³, Aldino Javier Saviola^{1*}

¹Department of Chemistry, Faculty of Mathematics and Natural Sciences, Universitas Gadjah Mada, Yogyakarta 55281, Indonesia.

²Research Center for Chemistry, National Research and Innovation Agency (BRIN), The B. J. Habibie Science and Technology Area, South Tangerang, Banten 15314, Indonesia.

³Department of Geographic Information Science, Faculty of Geography, Universitas Gadjah Mada, Yogyakarta 55281, Indonesia.

Received: 14th October 2024; Revised: 28th November 2024; Accepted: 28th November 2024 Available online: 3rd November 2024; Published regularly: December 2024



Abstract

Pharmaceutical industrial wastewater frequently contains high amounts of phenolic substances, which pose severe threats to the ecosystem and human health. Therefore, efficient removal of these pollutants is urgently needed. In the present work, sulfated Lapindo mud (SLM) was prepared using the sonochemical method and applied as an adsorbent for phenol removal in aqueous media and actual wastewater samples from Code River, Yogyakarta. Modification of Lapindo mud (LM) using sulfuric acid enables it to remove its impurities, resulting in a material containing 78.4% silica (SiO₂) and 15.3% alumina (Al₂O₃). The SLM adsorbent demonstrated sufficient adsorption performance of 49.8% with an optimal initial phenol concentration of 120 mg/L with a contact time of 100 min at pH of 10. The maximum adsorption capacity (qmax) obtained by the Langmuir isotherm model was 27.2 mg/g. The adsorption process follows pseudo-second-order because it has two active sites, Brønsted acid sites (–SiOH and –SO₃H) and Lewis acid sites (Si⁴⁺). Phenol in base condition undergoes a deprotonation reaction that is stabilized by the acid-active sites of the SLM adsorbent through intermolecular forces. Considering the large adsorption capacity and quick kinetic, the SLM adsorbent can be a promising cheap and green material to remove phenolic substances in wastewater, especially in the river near the medical facility.

Copyright © 2024 by Authors, Published by BCREC Publishing Group. This is an open access article under the CC BY-SA License (https://creativecommons.org/licenses/by-sa/4.0).

Keywords: Adsorption; phenol; Lapindo mud; sulfation; sonochemical method

How to Cite: Wijaya, K., Bhagaskara, A., Sani, M.F.M., Vebryana, M.F., Pratama, F.A., Anggraeni, W., Amin, A.K., Ramadhani, F.A., Saviola, A.J. (2024). Sonochemically Modified Lapindo Mud Using Sulfuric Acid for Efficient Adsorption of Phenol in Aqueous Media and Real Wastewater Samples. Bulletin of Chemical Reaction Engineering & Catalysis, 19 (4), 635-648 (doi: 10.9767/bcrec.20228)

Permalink/DOI: https://doi.org/10.9767/bcrec.20228

1. Introduction

The Lapindo mud (LM) disaster occurred on May 29, 2006, in Sidoarjo, Indonesia, resulting in extensive environmental, anthropogenic, and material damage, submerging 1,071 hectares of land. LM contains a variety of volcanic substances

with high mineral content. Chemical analyses indicate silica (SiO₂) is the predominant mineral, constituting 53.03%, suggesting its potential as a silica resource in Indonesia [1]. Silica is widely utilized as a multifunctional material due to its unique physicochemical properties, biocompatibility, low toxicity, and large surface area [2]. Its surface area and pore structure are particularly advantageous for adsorption [3].

^{*} Corresponding Author. Email: aldino.javier@mail.ugm.ac.id (A.J. Saviola)

However, LM contains impurities that can block pores and reduce surface area, leaving only micropores on the material's surface. Materials with predominantly micropores face challenges in achieving efficient molecular diffusion [4]. Thus, a process to remove these impurities is essential.

The modification of LM through sulfation involves cleaning its surface and mitigating diffusion limitations. This process has been shown to enhance mass transfer while maintaining a large surface area during adsorption [5]. Such modifications have been successfully tested for the adsorption of CO₂ gas [6], drugs [7], dye waste [8], and spent metals [9]. Silica's structure, consisting of silicon bonded to four oxygen atoms, forms hydroxyl groups on its surface. It creates polarity, facilitating strong interactions with polar organic molecules via hydrogen bonds and dipole-dipole interactions.

In this study, sulfated Lapindo mud (SLM) was applied as an adsorbent to remove phenolic pollutants from pharmaceutical industrial wastewater. Phenols and their derivatives are moderately water-soluble pollutants commonly found in wastewater from various industries. These compounds are key raw materials for producing dyes, polymers, pharmaceuticals, and pesticides [10]. Specifically, phenolic compounds are used in the pharmaceutical industry as active ingredients in antipruritic, anti-inflammatory, and blemish-removal analgesic, products. However, their widespread use has led to significant environmental contamination, particularly in municipal and industrial wastewater treatment systems [11]. Phenol's welldocumented toxicity and ability to bioaccumulate significant environmental and health concerns. Phenol toxicity manifests in both acute and chronic forms. Acute exposure in humans can cause symptoms such as dryness in the throat and mouth, darkened urine (a result of lipid peroxidation), and systemic poisoning. Chronic exposure can lead to anorexia, muscle pain, headaches, gastrointestinal discomfort, and, ultimately, cancer. Phenol can also irritate the skin; prolonged dermal contact may cause severe damage. Oral ingestion of phenol, even in small amounts (as little as 1 gram), can result in severe liver and kidney damage or fatality [12].

Previous studies have explored phenol adsorption using various adsorbents, including coal [13], silica-based aerogels [14], high-silica zeolites [15], activated carbon [11], and biocharmodified layered double hydroxides [16]. In this study, we examined the potential of SLM as an adsorbent for phenol removal in aqueous media, including a case study using genuine wastewater samples from the Code River in Yogyakarta. According to Saraswati *et al.* [17], the midstream section of the Code River is polluted due to the presence of pharmaceutical, laundry, automotive, and livestock industries. The findings of this study

aim to highlight the potential of Lapindo mud as a sustainable adsorbent through a simple modification process, offering a promising solution for phenol removal and large-scale application in polluted water sources.

2. Materials and Methods

2.1 Materials

The materials and chemicals used in this study were Lapindo mud (LM), which was taken from a radius of \pm 800 m from the center of the mudflow in Porong, Sidoarjo, Indonesia; Folin-Ciocálteu reagent (FC), sulfuric acid (H₂SO₄, 98%), gallic acid (C₇H₆O₅), phenol (C₆H₅OH), sodium carbonate (Na₂CO₃), sodium hydroxide (NaOH), hydrochloric acid (HCl, 37%), and pyridine (C₅H₅N, 99%) were obtained from Merck; GF/F fiber filter paper (47 mm \times 0.7 µm; Whatman, Maidstone, UK) and deionized water were purchased from CV Fruitanol Energy.

2.2. Preparation of Lapindo Mud

Firstly, LM was washed using deionized water with a 1:3 (w/v) ratio and stirred at room temperature for 24 h at 500 rpm. After 24 h, the mixture was left overnight until the mud sediment was settled and the deionized water was replaced with the fresh one. This procedure was repeated until the pH of the wash water became neutral. The clean LM was filtered using filter paper to separate LM from the wash water, and then LM was dried overnight in the oven at 120 °C. The LM sample was calcined in a muffle furnace at 500 °C for 3 h. Then, the LM sample was sieved with a 100-mesh sieve.

2.3. Sulfation of Lapindo Mud

LM that has been washed was mixed with $\rm H_2SO_4~2~M$ at a ratio of 1:10 (w/v) and sonicated with an ultrasonic bath for 2 h at room temperature. The result of this process is called sulfated Lapindo mud (SLM). The SLM sample was washed using deionized water until pH became neutral and then dried in the oven at 120 °C overnight. Lastly, the SLM sample was calcined in a muffle furnace at 500 °C for 3 h and was sieved with a 100-mesh sieve.

2.4 Acidity Test of the Adsorbents

The acidity test of LM and SLM was conducted using the pyridine gravimetric method in a vacuum vessel. The process began with preparing a clean and empty porcelain crucible, which was then placed in an oven at 120 °C for 1 h and labeled as W_1 . Subsequently, 0.1 g of the sample was put into a porcelain crucible, heated in the oven at 120 °C for 1 h, and labeled as W_2 . The porcelain crucible containing the sample was then placed into the vacuum

vessel, closed tightly, and pyridine vapor was allowed to flow through. After 24 h, the vessel was opened, and the sample was immediately transferred to a desiccator. The crucible containing the sample was then labeled as W_3 . The acidity of the material (mmol.g-1 pyridine) was determined using the following Equation (1).

$$Acidity = \frac{(W_3 - W_2)}{(W_2 - W_1)MW_{pyridine}} \times 1000 \ mmol/g \tag{1}$$

2.5. Adsorbents Characterizations

X-ray Fluorescence Spectrometer Bruker, 50 kV, 50 mA, USA) determined the mineral content in LM and SLM samples. The functional group identification was carried out using a Fourier Transform Infrared Spectrometer (FTIR, Shimadzu 82010C, wavenumber = 400-4000 cm⁻¹, resolution = 4cm⁻¹, 32 scans, Japan). The mineral content and crystallinity change analysis of the material was also analyzed by X-ray Diffractometer (XRD, PANanalytical Empyrean, 40 kV, 40 mA, Cu-Kα = $1.54 \text{ Å}, 2\theta = 10-80^{\circ}, \text{ USA}$). The Surface Area Analyzer (SAA, Micromeritics Gemini VII Version 5.03) instrument studied each adsorbent's surface area and pore characteristics with a degassing temperature of 300 °C for 3 h. The morphological and elemental composition study was analyzed using a Scanning Electron Microscope coupled with a Field Emission Scanning Electron Microscope-Dispersive X-ray spectrometer instrument (FESEM-EDX Mapping, JEOL JSM-6510LA).

2.6. Phenol Adsorption Study

The adsorption experiments were conducted in a batch container with a stirrer. The experimental setup is shown in Figure 1. Phenolic substances were determined using gallic acid as the standard solution and indicator consisting of FC reagent that is diluted 10 times and sodium carbonate solution (Na₂CO₃, 7.5%). Α spectrophotometric method measured phenolic compound using an ultraviolet-visible spectrometer (UV-Vis, Orion Aguamate 8100, λ = 760 nm). Wavelength was obtained from the UV-Vis spectrum at various gallic acid standard solution concentrations. Several parameters significantly influence the phenol adsorption process using the SLM adsorbent. In this research, the parameters tested are an acid-base condition of phenol solution, adsorption time (kinetics), temperature adsorption, concentration of phenolic substances to determine adsorption isotherm models. The adsorption capacities $(q_t, mg/g)$ and percent adsorption (R, %)of the phenolic compound at equilibrium are calculated with Equations (2) and (3):

$$q_{t} = \frac{(c_0 - c_t)V}{m} \tag{2}$$

$$q_{t} = \frac{(c_{0} - c_{t}) V}{m}$$

$$R = \frac{c_{0} - c_{e}}{c_{0}} \times 100\%$$
(2)

where, q_t (mg/g) is the phenolic compound's adsorption capacity at time t (min), C_0 and C_e (mg/L) are the phenolic compound's initial and equilibrium concentrations, respectively, V(L) is the solution's total volume, and m (g) is the SLM's

2.6.1 Optimization of the phenol adsorption conditions

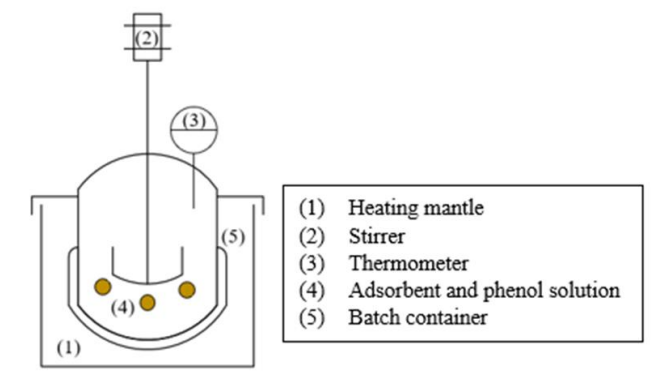
Firstly, 150 mg SLM was added 25 mL of 150 ppm phenol solution under acid, neutral, and base conditions. A 25 mL of 0.5 M HCl solution was used to create an acid condition; for neutral conditions, 25 mL of deionized water was used, and 25 mL of 0.5 M NaOH solution was used for base conditions. The mixture of SLM and phenol solution was then separated using vacuum filtration. The filtrated product was added with FC reagent and tested using a UV-Vis instrument. The optimal conditions are then re-evaluated by expanding the pH range under those conditions.

2.6.2 Adsorption kinetics and thermodynamic study

Adsorption kinetics studies were conducted at contact times of 10, 15, 30, 45, 60, 100, and 120 min. The adsorption process was performed at room temperature and optimum conditions. The adsorption kinetics were studied using two kinetic models: pseudo-first-order kinetics (Lagergren) pseudo-second-order kinetics (Ho and and McKay). Meanwhile, for thermodynamic calculation, we use a variation of temperature. The adsorption process was conducted with the temperature variation (30, 40, and 50 °C) in phenol solution.

2.6.3 Adsorption isotherm models

Adsorption isotherm models were determined at various phenolic compound concentrations of



phenol Figure 1. Experimental set-up foradsorption process.

20, 40, 60, 80, 100, and 120 ppm. The adsorption process was performed at room temperature and optimum conditions. Adsorption isotherm phenolic compounds were determined using Freundlich, Langmuir, and Temkin models.

2.6.4 Application of the SLM adsorbent in Code River's water samples

Based on the natural environmental conditions and the overall layout of the sub-urban planning, we use the grab sampling method to collect water samples around the Code River. A total of 5 sampling sites along the midstream Code River were selected for this sample collection. The sample distribution is shown in Figure 2. We choose only the midstream because of the limited distance from the medical facility to the river. All samples were collected on February 10 and 11, 2024. Global positioning system (GPS) was used to locate the sampling stations during the sampling process. Water samples were taken 50 cm below the surface level in each sampling site with 4 L pre-cleaned polyethylene bottles. All water samples were transported to the laboratory directly after sampling and kept at 4 °C before analysis. For the following steps, the samples were filtered using filter paper in vacuum filtration to reduce the amount of sedimentation in the samples. The phenol in the filtrate was then

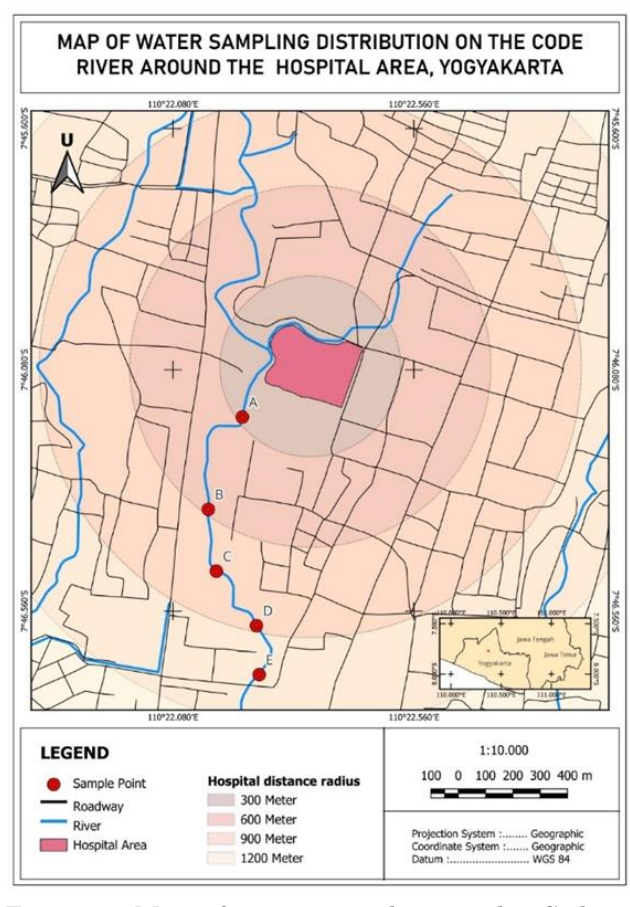


Figure 2. Map of water sampling in the Code River, Yogyakarta

analyzed using FC methods and a UV-Vis instrument.

3. Results and Discussion

3.1. XRF Analysis

Lapindo mud (LM) and sulfated Lapindo mud using (SLM) characterized were X-rav fluorescence (XRF) to determine their elemental composition in the form of oxide compounds. The results, shown in Figure 3, reveal that silica (SiO₂) and alumina (Al₂O₃) are the primary components of the LM and SLM samples, highlighting their potential as adsorbent materials for wastewater treatment. Impurities, such as hematite (Fe₂O₃), calcium oxide (CaO), and other minerals, were also identified. These impurities likely originated from the sedimentation of rocks and mud near the Lapindo mudflow and from surrounding farmland [18]. Treatment with sulfuric acid, through processes such as dealumination and demineralization, successfully reduced these impurities [19]. Consequently, the Si/Al ratio increased from 2.60 in LM to 4.24 in SLM. The removal of impurities enhances the adsorption performance of Lapindo mud, particularly for phenol, further underscoring the significance of these findings.

3.2. XRD Analysis

The mineral composition and crystallinity of LM and SLM were further analyzed using X-ray diffraction (XRD), with the resulting diffractograms presented in Figure 4. The primary peaks correspond to silica (S) (ICDD No. 96-900-5021) in quartz minerals and alumina (A) (ICDD No. 96-901-5977) in corundum minerals. These findings align with the XRF data, confirming that SiO2 and Al2O3 are the dominant mineral components in Lapindo mud [1,20]. Additionally, peaks for impurities such as magnetite (F) and calcium oxide (C) were observed in the LM samples. These impurities, located on the surface of the mud, block the active adsorption

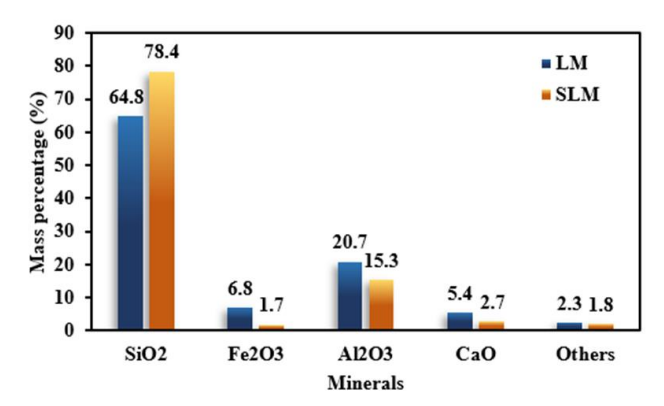


Figure 3. Element composition of the LM and SLM samples obtained by XRF

sites and reduce adsorption capacity. After sulfuric acid treatment, the impurity peaks disappeared in the SLM diffractogram, indicating their removal. The sonochemical method employed during this treatment effectively produced SLM materials with significantly fewer impurities.

Sulfuric acid treatment also increased the degree of crystallinity of the LM samples, from 18.71% to 39.76% in the SLM samples. This improvement is attributed directly to the treatment, which enhances the specific surface area and active site distribution of the adsorbent materials, which are critical factors for effective adsorption.

3.3. FTIR Study

The Fourier-transform infrared (FTIR) spectra of LM and SLM are shown in Figure 5. A broad absorption peak in the 900–1100 cm⁻¹ region indicates overlapping vibrations. The peak at 1000–1100 cm⁻¹ corresponds to the asymmetric

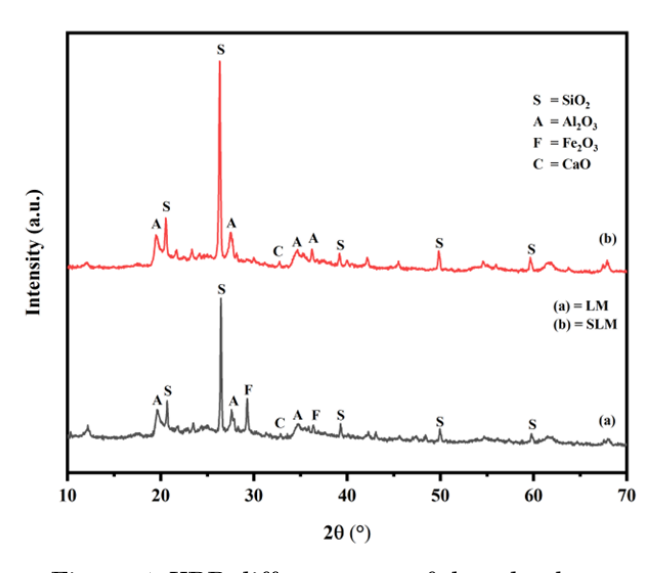


Figure 4. XRD diffractogram of the adsorbents

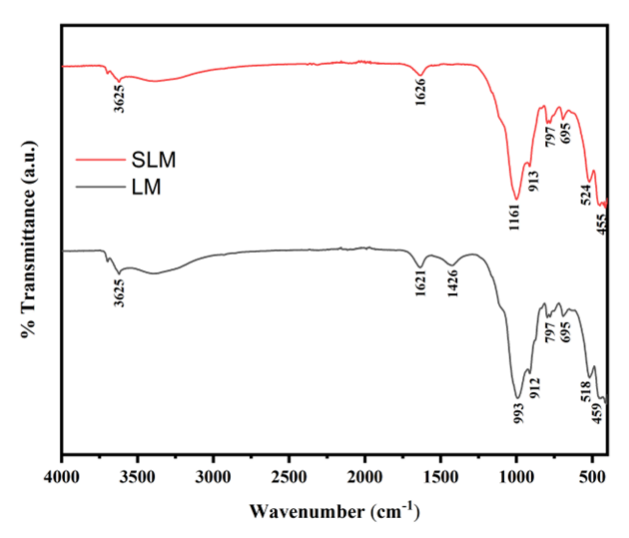


Figure 5. FTIR spectra of the adsorbents

stretching vibration of the Si–O–X framework bond (X = Si or Al) [21], while the 900–1000 cm⁻¹ peak represents the symmetric stretching vibration of bisulfate groups (HSO₄⁻) attached to the silica surface, forming a sulfated silica structure [22]. Peaks in the 450–800 cm⁻¹ range are attributed to the bending vibration of the Si–O–X framework bond [23,24]. Additionally, a peak around 3600 cm⁻¹ corresponds to the stretching vibration of hydroxyl (–OH) groups, originating from water adsorbed onto the materials or silanol and aluminol groups. The absorption around 1600 cm⁻¹ represents the bending vibration of –OH groups.

During the sulfation process, Lapindo mud undergoes dealumination and demineralization, which release aluminum and other mineral cations that cover the active sites of the mud. The sulfate anion (SO₄²·) plays a critical role as a ligand, donating free electron pairs from its oxygen atoms to form coordination bonds with Si⁴⁺ cations [25]. This process, coupled with the extraction of impurities, facilitates the formation of a sulfated silica polymer on the Lapindo mud's surface, as depicted in Figure 6. These modifications enhance the material's properties, including an increased Si/Al ratio, improved porosity, and augmented specific surface area, making SLM a more effective adsorbent [26].

3.4. Acidity Study

The acid sites on the adsorbent are categorized into Brønsted and Lewis acid sites, which serve as active sites for phenol adsorption onto the adsorbent's surface. On the surface of Lapindo mud (LM), hydroxyl groups in sulfate (S–OH) and silanol groups (Si–OH) act as Brønsted acid sites, while silica cations (Si⁴⁺) function as Lewis acid sites. A noticeable increase in acidity is observed when comparing LM to sulfated Lapindo mud (SLM) (see Table 1). Higher acidity values indicate a greater number of acid sites on the surface of the adsorbent. This increase occurs as cationic impurities are removed, allowing more H⁺ ion exchanges from the sulfate

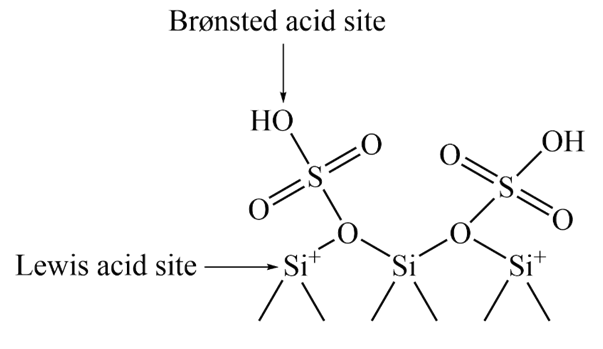


Figure 6. Hypothetic structure of sulfated silica in the SLM adsorbent

anion bonded to silica cations. This exchange creates additional Brønsted acid sites within the silica matrix and facilitates the formation of more accessible pores, increasing the number of Lewis acid sites. The sonochemical method, employing ultrasonic baths, further enhances this process by generating "cavitation bubbles"—small, transient gas bubbles that form and collapse in a liquid under sound waves [27]. This effect provides optimal energy throughout the system, ensuring efficient sulfation of Lapindo mud.

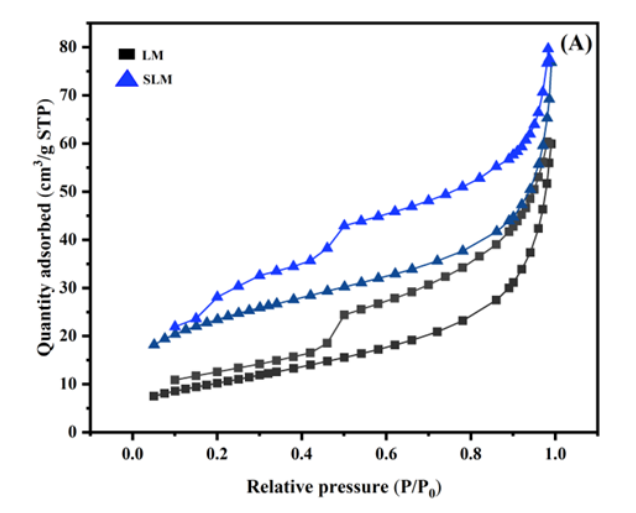
3.5. Surface and Pore Characteristics

The nitrogen (N_2) adsorption-desorption isotherm curves of LM and SLM, shown in Figure 7(a), exhibit type IV behavior according to IUPAC classification, indicative of mesoporous materials with pore sizes in the range of 2 < d < 50 nm. This confirms the successful production of mesoporous silica from Lapindo mud using the sonochemical method.

The SLM sample displays a more pronounced and expanded hysteresis loop, particularly at higher relative pressures (P/P_0 approaching 1.0), compared to LM. This suggests the treatment effectively enhanced the mesoporous structure, with increased pore size and volume, resulting in improved adsorption characteristics. In contrast, the LM sample exhibits a less pronounced hysteresis loop and a gradual adsorption curve, indicating less-developed mesopores in the untreated material. While both samples contain mesopores, the larger and more open hysteresis loop in the SLM sample confirms the

Table 1. Acidity value of the adsorbents

Sample	Acidity (mmol/g pyridine)
LM	0.50
SLM	4.25



enhancement of the mesoporous structure through sonochemical treatment.

Both samples exhibit minimal adsorption at low relative pressures ($P/P_0 < 0.01$), indicating a negligible presence of micropores. As the relative pressure increases to $P/P_0 \sim 0.5$, a plateau with hysteresis is observed, suggesting multilayer formation and capillary condensation mesoporous and macroporous structures [28]. Additionally, the significant increase P/P_0 close adsorption volume at 1 is characteristic of macropores within aluminosilicate aggregates [29]. The pore size distribution curves, depicted in Figure 7(b), further confirm the presence of mesopores in the 2–14 nm range.

The textural properties of LM and SLM are summarized in Table 2. The SLM sample exhibits higher specific surface area and pore volume than LM, attributed to the reduction of mineral impurities covering its pores during the sulfation process. However, uneven distribution of sulfate groups on the silica matrix surface during the calcination process may result in a decrease in pore diameter, likely caused by particle agglomeration on the surface of the SLM adsorbent.

3.6 Morphological and Elemental Content Analysis

Field-emission scanning electron microscopy (FESEM) micrographs of LM and SLM, shown in Figure 8, illustrate the morphological changes in the materials. LM displays a non-uniform particle

Table 2. Textural properties of the adsorbents

Sample	Specific surface area	Total pore volume	Average pore diameter (nm)
	$(m^2.g^{-1})$	$(cm^3.g^{-1})$	
LM	37.01	0.092	9.91
SLM	78.06	0.118	6.03

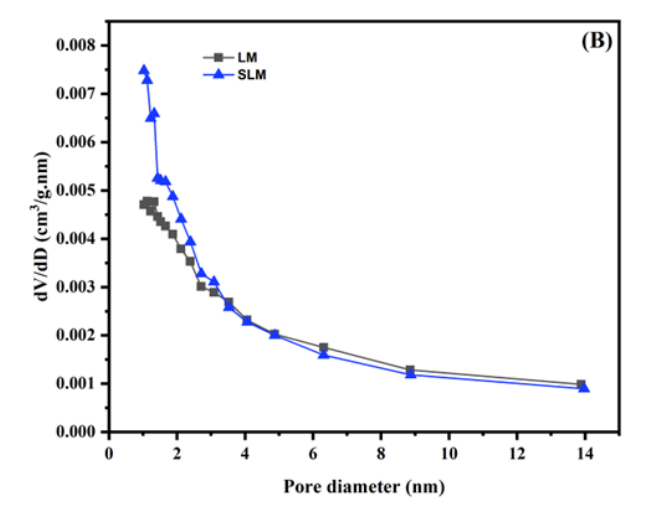


Figure 7. (a) N₂ adsorption-desorption isotherm profiles and (b) pore diameter distribution curves of the adsorbents

size, while the addition of sulfuric acid induces particle aggregation and increases particle size. The acid treatment also results in a cleaner surface for the SLM adsorbent, enhancing its specific surface area and adsorption capacity. These improvements make SLM more effective for phenol adsorption applications, as the removal of impurities and the creation of additional active sites significantly enhance its performance.

The results of the energy-dispersive X-ray (EDX) analysis, used to determine the elemental composition of the adsorbent materials, are presented in Table 3. The LM sample contains significant impurities, including alkaline earth elements and various metals. These impurities are significantly reduced following the addition of sulfuric acid. The EDX results reveal a dealumination phenomenon, evidenced by a decrease in aluminum content. The Si/Al ratio of

the SLM sample increases from 2.43 to 4.17, confirming the removal of aluminum and other impurities. Additionally, the successful sulfation process is verified by the detection of sulfur elements in the SLM sample.

3.6 Phenol Adsorption Study

3.6.1 Acid-base condition of phenol adsorption process using the SLM adsorbent

The acid-base conditions of the system play a critical role in determining the adsorption efficiency of phenol on the SLM material. As shown in Figures 9(a) and (b), basic conditions, particularly at pH of 10, yield significantly higher adsorption than acidic or neutral conditions. This is attributed to the deprotonation of phenol's hydroxyl group in basic environments, forming the phenolate ion, a conjugate base of phenol. This

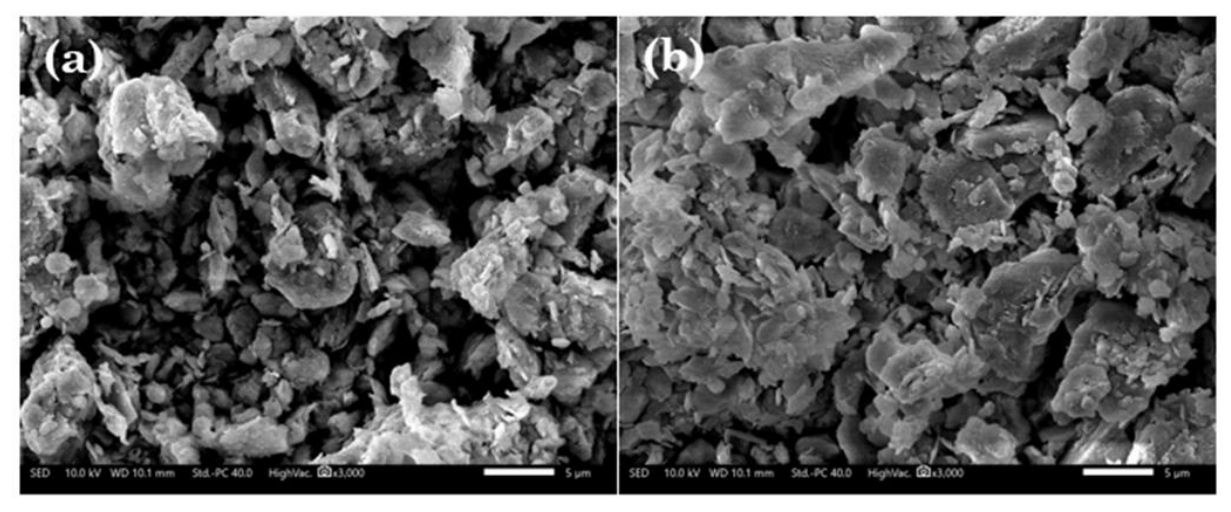


Figure 8. FESEM images of (a) LM and (b) SLM at 3,000 times magnification

Table 3. Elemental composition of the adsorbents obtained by EDX (nd: not detected)

Cample		Eleme	ent content (v	vt%)			
Sample	Si	Al	О	S	Mg	Ca	Fe
LM	22.14	9.11	61.95	nd	1.10	1.75	3.95
SLM	27.25	6.53	62.94	3.28	nd	nd	nd

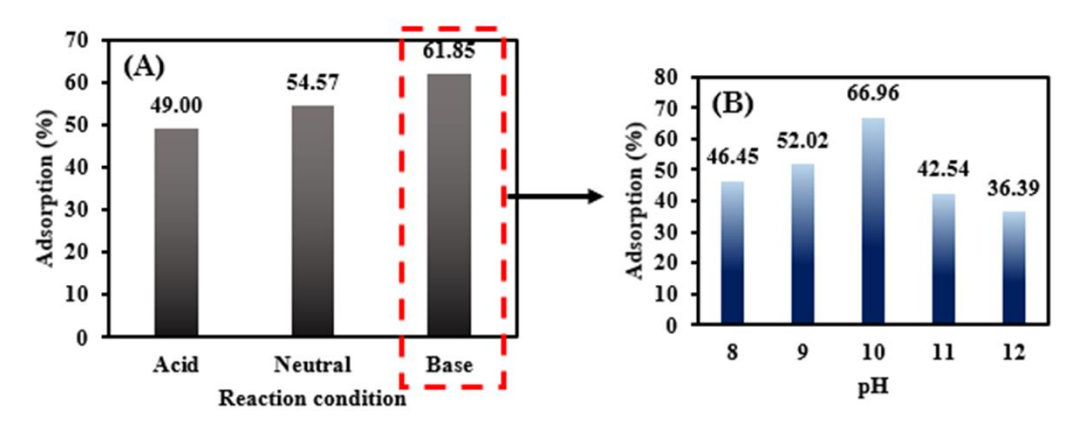


Figure 9. (a) Percent adsorption of phenol with different conditions using the SLM adsorbent and (b) extrapolate in base condition

transformation increases the phenol's pKa from 10.00 to 10.50 [30]. The phenolate ion is readily adsorbed onto the acid sites of the SLM surface. It interacts with Brønsted acid sites via hydrogen bonding with the sulfate group or with Lewis acid sites through ionic interactions with silica cations. In acidic and neutral conditions, phenol remains a $\sim 9.98 - 10.00$), weak acid (pKa where deprotonation occurs less frequently, reducing its adsorption efficiency. Figure 10 illustrates the deprotonation reaction and the phenol adsorption process on the SLM adsorbent.

3.6.2 Adsorption kinetics and isotherms of phenol adsorption

The adsorption kinetics were investigated using pseudo-first-order (Equation 4) and pseudo-second-order (Equation 5) models. Figure 11 depicts the effect of contact time on the adsorption process. Maximum adsorption efficiency (88.52%) was achieved within 100 min. The limiting factors in the 10 to 100 min range include saturation of active sites, intraparticle diffusion, and chemical interactions. The initial rapid adsorption phase is followed by slower diffusion of phenol molecules into the pores, with a gradual decline in

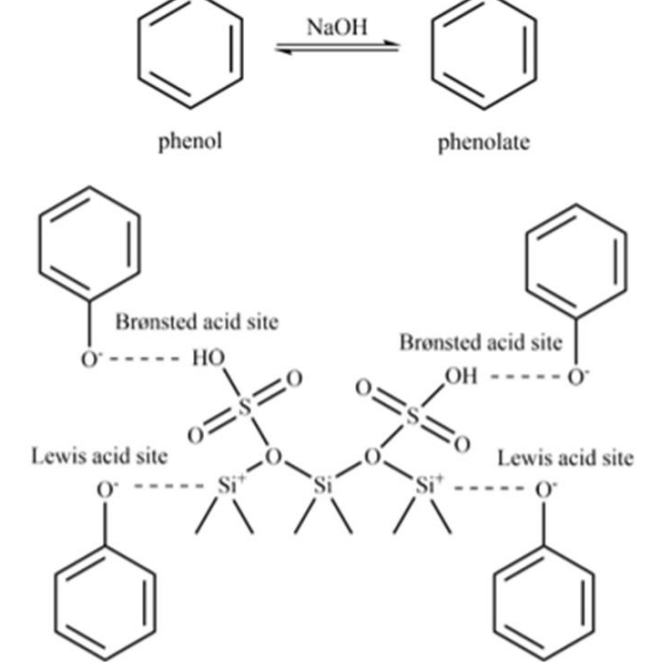
adsorption rate as active sites are occupied. Due to the reduced availability of unoccupied sites, chemical interactions between phenol and active sites on the adsorbent also slow over time.

Adsorption efficiency increased with contact time but declined slightly at 120 min as the adsorbent reached saturation. This decline may result from competitive interactions among adsorbed molecules. As saturation approaches, weaker interactions (e.g. van der Waals forces) may be disrupted, causing partial desorption of phenol back into the solution. Re-equilibrium dynamics, where adsorption and desorption achieve a balance, could also explain the reduction in efficiency. Additionally, prolonged exposure to phenol solution may cause minor structural damage to the adsorbent material.

Table 4 presents the results of the kinetics parameters of phenolic adsorption on the SLM adsorbent. The adsorption process of the phenol compound on the SLM adsorbent followed a pseudo-second-order adsorption kinetics model (Ho and McKay) with a linear regression value of 0.99976. The pseudo-second-order kinetic model reveals that the adsorption kinetics is significantly influenced by two active sites, the

Table 4. Kinetic parameters of phenol adsorption using the SLM adsorbent

Pseudo-first-order			Pse	eudo-second-order	
k_1 (min ⁻¹)	$q_{ m e}$ (mg.g ⁻¹)	\mathbb{R}^2	$k_2 (\mathrm{mg.g^{\text{-}1}.min^{\text{-}1}}) \qquad \qquad q_{\mathrm{e}} (\mathrm{mg.g^{\text{-}1}}) \qquad \qquad \mathrm{R}$		
-0.0062	1.251	0.824	0.0338	29.56	0.9998



OH

Figure 10. (a) Deprotonation reaction of phenol and (b) adsorption of phenol on the SLM material

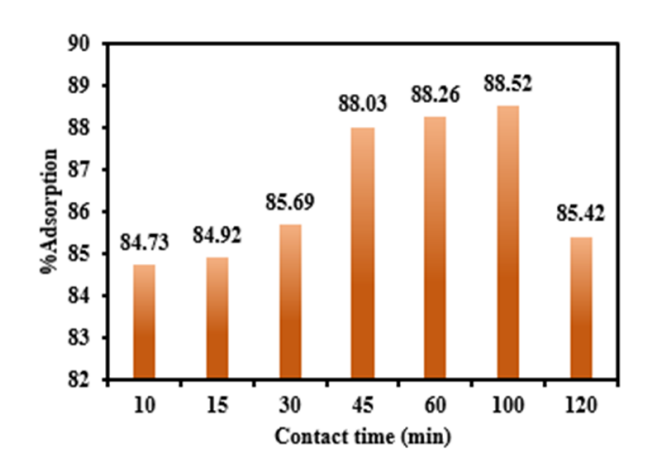


Figure 11. Variation of contact time in phenol adsorption process using the SLM adsorbent

Brønsted (-SO₃H) and Lewis acid site (Si⁴⁺), as shown in Figure 10. The rate constant value obtained for phenolic adsorption was 0.0338 mg.g-1.min-1, and the adsorption capacity was 29.56 $mg.g^{-1}$.

Pseudo-first-order equation:

$$\log(q_e - q_t) = \log(q_e) - K_1 t$$
(4)

$$\frac{t}{q_{\rm t}} = \frac{1}{K_2 q_{\rm e}^2} + \frac{t}{q_{\rm e}} \tag{5}$$

where, $q_{\rm t}$ and $q_{\rm e}$ (mg.g-1) represent the phenolic compound adsorption capacity at time t (min) and equilibrium, respectively. k_1 (min⁻¹) and k_2 (mg.g⁻¹ ¹.min⁻¹) are the corresponding rate constants.

The effect of phenol concentration adsorption capacity is utilized to optimize the adsorption process, which aims to determine the optimum adsorbate concentration. The initial phenol concentration was varied to 20, 40, 60, 80, 100, and 120 ppm. The adsorption process was best performed in base condition, 100 min of contact time, and different initial phenol concentrations. The effect of the initial adsorbate concentration on the adsorption of phenol using the SLM adsorbent is shown in Figure 12.

Figure 12 demonstrates that the initial concentration of phenol directly influences the adsorption capacity of the SLM adsorbent. Adsorption capacity increases with higher initial concentrations, reaching a maximum at 120 ppm. At 100 ppm, both adsorption efficiency and capacity are optimal, with 49.8% of phenol (at an initial concentration of 120 mg/L) removed within

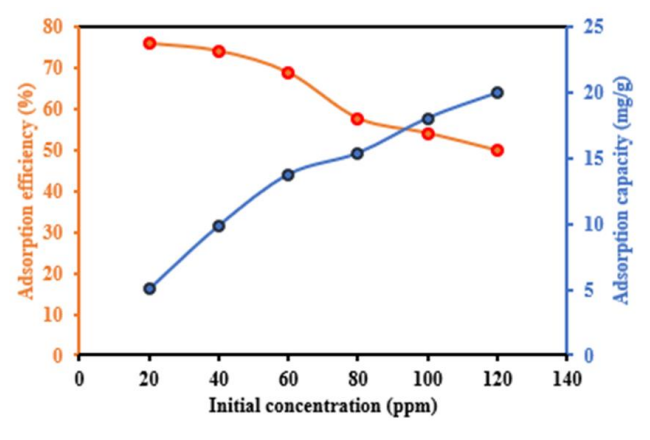


Figure 12. Adsorption efficiency and capacity of phenol adsorption process using the SLM adsorbent

100 min. The increasing adsorption capacity suggests that the phenol adsorption process adheres to the Langmuir isotherm model (Equations 6 and 7) rather than the Freundlich (Equation 8) or Temkin (Equation 9) models. The Langmuir model indicates a plateau or saturation in adsorption capacity, consistent with the observed data [30]. The parameters of the adsorption isotherm models for phenol adsorption on SLM are summarized in Table 5. The findings support the Langmuir model as the most suitable representation of the adsorption process, indicating monolayer adsorption homogeneous surface with finite active sites.

Langmuir isotherm model:

Langmuir isotherm model:
$$\frac{1}{q_e} = \left(\frac{1}{C_e} \times \frac{1}{K_L q_{\text{max}}}\right) + \frac{1}{q_{\text{max}}}$$

$$R_L = \frac{1}{1 + K_L C_0}$$
(6)

$$R_{\rm L} = \frac{1}{1 + K_{\rm L} C_0} \tag{7}$$

Freundlich isotherm model:

$$\log q_{\rm e} = \log K_{\rm f} + \frac{1}{n} \log C_{\rm e} \tag{8}$$

Temkin isotherm model:

$$q_{\rm e} = \left(\frac{RT}{b_{\rm T}}\right) \ln A_{\rm T} + \left(\frac{RT}{b_{\rm T}}\right) \ln C_{\rm e} \tag{9}$$

where, the K_L (L.mg⁻¹) is the Langmuir constant, $R_{\rm L}$ is separation factor, $K_{\rm f}$ (L.g⁻¹) is the Freundlich constant, A_T (L.g⁻¹) is the Temkin isotherm constant, $b_{\rm T}$ is Temkin energy constant (J.mol⁻¹), R is a ideal gas constant (8.314 J.K⁻¹.mol⁻¹), T is temperature in Kelvin, and q_{max} is maximum adsorption capacity (mg.g-1).

The phenol adsorption isotherm follows the Langmuir model, assuming that the active group on the surface of SLM is homogenous and forms a monolayer with the type of chemical bonding (chemisorption). From Table 5, the large q_{max} and $K_{\rm L}$ values were obtained at 27.17 mg.g⁻¹ and 0.05 L.mg⁻¹. A higher indicates a higher capacity for SLM when adsorbing phenol compound. The R_L values indicate the adsorption as unfavorable when $R_L > 1$, linear when $R_L = 1$, favorable when $0 < R_{\rm L} < 1$, and irreversible when $R_{\rm L} = 0$. The data indicates that the value for phenol adsorption on the SLM surface is 0.20, which suggests that the adsorption process is favorable.

After identifying the optimal conditions for phenol adsorption (pH = 10, initial phenol concentration of 100 ppm, and contact time of 100 min), a performance comparison between LM and SLM adsorbents was conducted. The adsorption

Table 5. Adsorption isotherm model and parameters of phenol adsorption using the SLM

Freundl	ich		Langmuii	•			Temkin		
K _F (L.g ⁻¹)	n	R^2	$K_{ m L}$ (L.mg ⁻¹)	$q_{ m max} \ ({ m mg.g^{ ext{-}1}})$	$R_{ m L}$	R^2	$K_{ m T}$ (L.g ⁻¹)	$b_{ m T}$ (J.mol $^{-1}$)	R^2
1.52	1.96	0.9455	0.05	27.17	0.20	0.9906	5.658	0.53	0.9883

efficiencies are summarized in Table 6. The results demonstrate that surface modification with sulfate groups significantly enhances phenol adsorption efficiency. This improvement is attributed to the introduction of Brønsted acid sites provided by sulfate groups, whereas the unmodified LM adsorbent relies solely on Lewis acid sites represented by silica cations.

3.6.3 Thermodynamics of phenol adsorption process

The mechanism of the adsorption process can from the thermodynamic determined parameters: free energy (ΔG°), enthalpy (ΔH°), and entropy (ΔS°). The graphic plot of ln (k_2/T) versus 1/T is linear, indicated by the R^2 value close to 1 in Figure 13. The values of ΔH° and ΔS° are obtained from the slope and intercept of the Eyring-Polanyi equation (see Equation 10 and 11) and Gibbs-Duhem equation (see Equation 12), where ΔG° at various temperatures is shown in Table 7. The ΔG° values negative indicates that the process is spontaneous. Negative values for ΔH° and positive values for ΔS° indicate that the phenol adsorption process on the SLM material takes place exothermically with increased irregularities on the surface.

Eyring-Polanyi equation:

$$k = \frac{k_{\rm B}}{h} \times e^{\left(\frac{\Delta H}{RT}\right)}$$

$$\ln\left(\frac{k}{T}\right) = -\left(\frac{\Delta H}{RT}\right) + \ln\left(\frac{k_{\rm B}}{h}\right) + \frac{\Delta S}{R}$$
(10)

$$\ln\left(\frac{k}{T}\right) = -\left(\frac{\Delta H}{RT}\right) + \ln\left(\frac{k_{\rm B}}{h}\right) + \frac{\Delta S}{R} \tag{11}$$

Gibbs-Duhem equation:

$$\Delta G = \Delta H - T\Delta S$$
 (12)

3.6.4 Application of the SLM adsorbent in Code River's water samples

The SLM adsorbent was further applied to wastewater samples collected from the Code River, Yogyakarta. Sampling was conducted at five different points near healthcare facilities and residential areas, strategically chosen for their potential contributions to phenolic compound contamination. Table 8 presents the effectiveness of the SLM adsorbent in reducing phenol levels from these sampling points. The adsorption process was conducted under optimal conditions (100 min at pH of 10) using 150 mg of SLM. Prior to adsorption, the pH of the river samples was adjusted from 8.5 to 10 using a weak base solution. Among the sampling points, Point E exhibited the highest reduction in phenol levels. The results indicate that phenolic compound

Table 8. Phenols adsorption in Code River's water samples using the SLM adsorbent

Sample	Coordinate (South Latitude, East Longitude)	Distance from medical facility (m)	Initial concentration (ppm)	Adsorption (%)
A	(-7.769483, 110.370281)	20	8.07	38.51
В	(-7.772562, 110.369156)	370	7.30	46.67
\mathbf{C}	(-7.774661, 110.369435)	630	6.07	60.16
D	(-7.776439, 110.370776)	870	5.84	79.39
\mathbf{E}	(-7.777965, 110.370947)	1120	5.27	82.20

Table 6. Performance comparison of LM and SLM adsorbent

Adsorbent	Adsorption efficiency \pm SD
LM	40.71 ± 0.64
SLM	76.34 ± 0.29

Table 7. Thermodynamic parameters of phenol adsorption process using the SLM adsorbent

1/T (K-1)	0.0033	0.00319	0.00309
$\ln (k_2/T)$	5.957	7.399	8.632
$q_{ m e}$ (mg/g)	29.56	65.75	84.60
\mathbb{R}^2		0.9993	
T(K)	303.15	313.15	323.15
$\Delta G^{\circ} (kJ/mol)$	-173.16	-175.28	-177.40
$\Delta H^{\circ} (kJ/mol)$		-108.99	
ΔS° (J/K.mol)		0.2117	

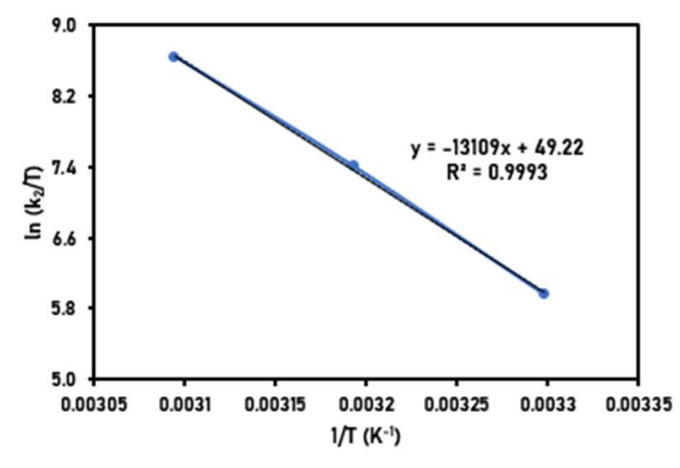


Figure 13. The graphic plot of Eyring-Polanyi equation

concentrations decrease with increasing distance from the contamination source, enhancing adsorption efficiency. These findings highlight the potential of SLM as a promising solution for mitigating phenolic contamination in water bodies.

Thermal regeneration was employed as an effective method to restore the sulfated Lapindo Mud (SLM) adsorbent after phenolic compound adsorption. This process involves heating the spent SLM to temperatures between 300 and 500 °C, enabling the desorption or decomposition of captured phenolic compounds. The thermal treatment regenerates the SLM, restoring its adsorption capacity for reuse. This method offers significant advantages, including controlled removal of phenolic compounds and reduced environmental impact when performed in a controlled environment, such as a furnace or reactor. Adherence to environmental regulations during thermal treatment is crucial to prevent the release of harmful gases. The regenerated SLM can be reused in subsequent adsorption cycles, enhancing process sustainability by minimizing waste and reducing the demand for new adsorbent materials.

3.6.5 Comparison of the adsorbent's effectiveness with results from previous studies

The findings of this study were compared with previous research on adsorbent materials, process conditions, and adsorption capacities, as summarized in Table 9. The comparison demonstrates that this study offers a more selective and effective process for phenol adsorption. Consequently, the results of this research present a viable approach for reducing phenol pollutants in water bodies, contributing to environmental conservation efforts.

4. Conclusion

In summary, the modification of Lapindo mud using sulfuric acid as an adsorbent demonstrated sufficient adsorption performance for phenols, realizing monolayer maximum adsorption capacities of 27.2 mg/g, according to the Langmuir isotherm model. With its swift adsorption of phenols, high silica content (78.40%), and the sulfate group layers, the SLM adsorbent is a promising candidate for wastewater treatment. The adsorption behaviors and capacities of phenol under different conditions, especially in pH, were highly related to their species in the solution (phenolate ion). Altogether, the results of this study revealed that the SLM is a highly suitable adsorbent material for removing phenol from wastewater, offering a potential solution to preserve the aquatic environment.

Acknowledgments

This research was fully supported by the facilities of the Physical Chemistry Laboratory, Department of Chemistry, Universitas Gadjah Mada, and the Radiation Laboratory Yogyakarta, the National Research and Innovation Agency (BRIN) Indonesia through *E-Layanan Sains* (ELSA).

CRediT Author Statement

Contributions: K. Wijaya: Conceptualization, Project Administration, Curation, Resources, Data Supervision, Validation, Writing, Review and Editing. A. Bhagaskara: Conceptualization, Methodology, Investigation, Formal Analysis, Data Curation, Writing Draft Preparation, Visualization, Software. M.F.M. Sani: Resources, Methodology, Investigation, Validation, Formal Analysis, Data Curation. M.F. Vebryana: Methodology,

Table 9. Comparison between phenol adsorbent's effectiveness from different literature

Adsorbent	Adsorption process conditions	Adsorption capacity (mg/g)	References
Sulfated Lapindo mud (SLM)	$C_0 = 120 \text{ mg/L}; 100 \text{ min}; 40 {}^{0}\text{C};$	27.2	This work
	pH of 10		
PSS-chitosan membrane	$C_0 = 1.0 \text{ mg/L}$; 100 min; pH of 8	3.97	[30]
Magnetic powder activated	$C_0 = 2.5 \ \mu \text{g/mL}; \ 120 \ \text{min}$	11.4	[31]
carbon (MPAC)			
Chitosan-CNT hydrogel	$C_0 = 40 \text{ mg/L}; 25 \text{ min}; 20 {}^{0}\text{C}; \text{pH}$	23.1	[32]
beads	of 7		
Covalent organic frameworks	$C_0 = 50 \text{ mg/L}; 35 \text{ min}; \text{ pH of } 5$	8.76	[33]
(COFs)			
NH_2 @COF	$C_0 = 0.1 \text{ mg/L}; 25 \text{ min}; \text{ pH of } 4$	12.5	[34]
Vinyl COF	$C_0 = 0.1 \text{ mg/L}; 5 \text{ min}; \text{ pH of } 4$	12.0	[34]
Leaves-generated biochar	Co = 1.5 mg/L; 120 min; pH of 11	21.3	[35]
Polyactic acid	140 °C; 45 min	22.3	[36]
(PLA-MPs)			

Investigation, Validation, Formal Analysis, Data Curation. W. Anggraeni: Methodology, Investigation, Validation, Formal Analysis, Data Curation. F.A.Pratama: Methodology, Investigation, Validation, Formal Analysis, Data Curation. A.K. Amin: Validation, Writing, Review and Editing, Data Curation. F.A. Ramadhani: Methodology, Investigation, Validation, Formal Analysis, Data Curation. A.J.Saviola: Project Administration, Conceptualization, Curation, Resources. Data Supervision, Validation, Writing, Review and Editing. All authors have read and agreed to the published version of the manuscript.

References

- [1] Rahmayanti, A., A'yuni, Q., Hartati, H., Purkan, P., Romanza, I.G. (2020). Synthesis and characterization of silica gel from Lapindo mud Sidoarjo. In IOP Conference Series: Earth and Environmental Science. 456, 012007. DOI: 10.1088/1755-1315/456/1/012007.
- [2] Tang, F., Li, L., Chen, D. (2012). Mesoporous silica nanoparticles: synthesis, biocompatibility and drug delivery. *Advanced Materials*. 24, 1504–1534. DOI: 10.1002/adma.201104763.
- [3] Samart, C., Prawingwong, P., Amnuaypanich, S., Zhang, H., Kajiyoshi, K., Reubroycharoen, P. (2014). Preparation of poly acrylic acid graftedmesoporous silica as pH responsive releasing material. Journal of Industrial and Engineering Chemistry. 20, 2153–2158. DOI: 10.1016/j.jiec.2013.09.045.
- [4] Numpilai, T., Muenmee, S., Witoon, T. (2016). Impact of pore characteristics of silica materials on loading capacity and release behavior of ibuprofen. *Materials Science and Engineering: C*. 59, 43–52. DOI: 10.1016/j.msec.2015.09.095.
- [5] Parlett, C.M.A., Wilson, K., Lee, A.F. (2013). Hierarchical porous materials: catalytic applications. *Chemical Society Reviews* 42, 3876–3893. DOI: 10.1039/C2CS35378D.
- [6] Witoon, T. (2012). Polyethyleneimine-loaded bimodal porous silica as low-cost and highcapacity sorbent for CO₂ capture. *Materials Chemistry and Physics*. 137, 235–245. DOI: 10.1016/j.matchemphys.2012.09.014.
- [7] Xu, X., Liu, Y., Wang, T., Ji, H., Chen, L., Li, S., Liu, W. (2019). Co-adsorption of ciprofloxacin and Cu(II) onto titanate nanotubes: speciation variation and metal-organic complexation. *Journal of Molecular Liquids*. 292, 111375. DOI: 10.1016/j.molliq.2019.111375.
- [8] Lei, X., Li, X., Ruan, Z., Zhang, T., Pan, F., Li, Q., Xia, D., Fu, J. (2018). Adsorption-photo-catalytic degradation of dye pollutant in water by graphite oxide grafted titanate nanotubes. *Journal of Molecular Liquids*. 266, 122–131. DOI: 10.1016/j.molliq.2018.06.053.

- [9] Liu, W., Wang, T., Borthwick, A.G.L., Wang, Y., Yin, X., Li, X., Ni, J. (2013). Adsorption of Pb²⁺, Cd²⁺, Cu²⁺ and Cr³⁺ onto titanate nanotubes: competition and effect of inorganic ions. *Science* of the Total Environment. 456, 171–180. DOI: 10.1016/j.scitotenv.2013.03.082.
- [10] Praveen, P., Loh, K.C. (20130. Trioctylphosphine oxide-impregnated hollow fiber membranes for removal of phenol from wastewater. *Journal of Membrane Science*. 437, 1–6. DOI: 10.1016/j.memsci.2013.02.057.
- [11] Mareai, B. M., Fayed, Aly, S.A., Elbarki, W.I. (2020). Performance comparison of phenol removal in pharmaceutical wastewater by activated sludge and extended aeration augmented with activated carbon. *Alexandria Engineering Journal*. 59, 5187–5196. DOI: 10.1016/j.aej.2020.09.048.
- [12] Gami, A.A., Shukor, M.Y., Khalil, K.A., Dahalan, F. A., Khalid, A., Ahmad, S.A. (2014). Phenol and its toxicity. *Journal of Environmental Microbiology and Toxicology*, 2, 11–24. DOI: 10.54987/jemat.v2i1.89.
- [13] Ahmaruzzaman, M., Sharma, D.K. (2005). Adsorption of phenols from wastewater. *Journal of Colloid and Interface Science*. 287, 14–24. DOI: 10.1016/j.jcis.2005.01.075.
- [14] Matias, T., Marques, J., Quina, M.J., Gando-Ferreira, L., Valente, A.J.M., Portugal, A., Duraes, L. (2015). Silica-based aerogels as adsorbents for phenol-derivative compounds. Colloids and Surfaces A: Physicochemical and Engineering Aspects. 480, 260–269. DOI: 10.1016/i.colsurfa.2015.01.074.
- [15] Jiang, N., Shang, R., Khalil, S.G.J. Heijman, F.A., L.C. Rietveld. (2020). Adsorption of triclosan, trichlorophenol, and phenol by highsilica zeolites: Adsorption efficiencies and mechanisms. Separation and Purification Technology. 235, 116152. DOI: 10.1016/i.seppur.2019.116152.
- [16] Amri, A., Rezonsi, R., Ahmad, N., Taher, T., Palapa, N. R., Mohadi, R., Lesbani, A. (2023). Biochar-Modified Layered Double Hydroxide for Highly Efficient on Phenol Adsorption. *Bulletin* of Chemical Reaction Engineering & Catalysis, 18, 460–472. DOI: 10.9767/bcrec.19898.
- [17] Saraswati, S.P., Ardion, M. V., Widodo, Y. H., Hadisusanto, S., 2019. Water Quality Index Performance for River Pollution Control Based on Better Ecological Point of View (A Case Study in Code, Winongo, Gadjah Wong Streams). Journal of the Civil Engineering Forum. 5, 47– 55. DOI: 10.22146/jcef.41165.
- [18] Rokhim, D.A., Islamiyah, K.K., Sanjaya, E.H. (2022). A review: analysis of metal and mineral content in the complexity of Sidoarjo hot mud as a source of renewable energy in Indonesia. *Journal of the Turkish Chemical Society*. 9, 1255–1262. DOI: 10.18596/jotcsa.1093763.

- [19] Wangsa, W., Saviola, A.J., Wijaya, K., Bhagaskara, A., Hauli, L., Saputra, D.A. (2024). Utilization of laboratory glove waste for fuel production through pyrolysis-hydrocracking consecutive process catalyzed by sulfated Indonesian natural zeolite. Reaction Kinetics, Mechanisms and Catalysis. 137, 1495—1514. DOI: 10.1007/s11144-024-02595-0.
- [20] Trisunaryanti, W., Triyono, T., Fallah, I.I., Salsiah, S., Alisha, G.D. (2022). Highly Selective Biohydrocarbon Production using Sidoarjo Mud Based Catalysts in the Hydrocracking of Waste Palm Cooking Oil. Bulletin of Chemical Reaction Engineering & Catalysis. 17, 712–724. DOI: 10.9767/bcrec.17.4.15472.712-724.
- [21] Paukshtis, E.A., Glazneva, T.S., Sadovskaya, E.M. Kaichev, V.V. (2019). Fiberglass fabrics as unusual catalytic materials: Features and applications. Journal of Mineral, Metal and Material Engineering. 5, 89–105. DOI: 10.31437/2414-2115/2019/05/11.
- [22] Ghoreishi, K., Asim, N., Yarmo, M., Samsudin, M. (2014). Mesoporous phosphated and sulphated silica as solid acid catalysts for glycerol acetylation. *Chemical Papers*. 68, 1199–1204. DOI: 10.2478/s11696-014-0550-x.
- [23] Trisunaryanti, W., Larasati, S., Bahri, S., Ni'mah, Y.L., Efiyanti, L., Amri, K., Nuryanto, R., Sumbogo, S.D. (2020). Performance comparison of Ni-Fe loaded on NH2-functionalized mesoporous silica and beach sand in hydrotreatment of waste palm cooking oil. *Journal of Environmental Chemical Engineering*. 8, 104477. DOI: 10.1016/j.jece.2020.104477.
- [24] Aneu, A., Wijaya, K., Syoufian, A. (2022). Porous silica modification with sulfuric acids and potassium fluorides as catalysts for biodiesel conversion from waste cooking oils. *Journal of Porous Materials*. 29, 1321–1335. DOI: 10.1007/s10934-022-01258-6.
- [25] Wijaya, K., Saputri, W. D., Aziz, I.T.A., Wangsa, Heraldy, E., Hakim, L., Utami, M. (2021). Mesoporous silica preparation using sodium bicarbonate as template and application of the silica for hydrocracking of used cooking oil into biofuel. Silicon. 14, 1583–1591. DOI: 10.1007/s12633-021-00946-3.

- [26] Ge, Y., Jia, Z., Gao, C., Gao, P., Zhao, L., Zhao, Y. (2014). Synthesis of mesoporous silica-alumina materials via ureatemplated sol-gel route and their catalytic performance for THF polymerization. Russian Journal of Physical Chemistry A. 88, 1650 1655. DOI: 10.1134/S0036024414100355.
- [27] Niasari, S. M., Esmaeili-Zare, M., Sobhani, A. (2012). Cubic HgSe nanoparticles: sonochemical synthesis and characterisation. *Micro & Nano Letters*. 7, 1300–1304. DOI: 10.1049/mnl.2012.0709.
- [28] Ramesh, K., Reddy, K.S., Rashmi, I., (2014).Biswas, A. K. Porosity distribution, surface area, and morphology of synthetic potassium zeolites: A SEM and N2 adsorption study. Communications In Soil Science and Plant Analysis. 45, 2171–2181. DOI: 10.1080/00103624.2014.929699.
- [29] Soboleva, T., Zhao, X., Malek, K., Xie, Z., Navessin, T., Holdcroft, S. (2010). On the micro-, meso-, and macroporous structures of polymer electrolyte membrane fuel cell catalyst layers. *ACS Applied Materials & Interfaces*. 2, 375–384. DOI: 10.1021/am900600y.
- [30] P., Pitsawong, W., Chenprakhon, Dhammaraj, Т., Medhanavyn, Sucharitakul, J., Tongsook, C., Miller, A. F. (2020). Tuning of pKa values activates substrates in flavin-dependent aromatic hydroxylases. Journal of Biological Chemistry. 295, 3965-3981. DOI: 10.1074/jbc.RA119.011884.
- [31] Nora, M., Bhagaskara, A., Agustisari, V., Lim, A., Alfalah, H.R., Siswanta, D. (2023). Fabrication of Polystyrene (PSS-Chitosan) Sulfonate-Chitosan Membrane as Dodecyl Benzene Sulfonate (DBS) Adsorbent in Laundry Wastewater. Jurnal Kimia Sains & Aplikasi. 26, 19-27.DOI: 10.14710/jksa.26.1.19-27.
- [32] Mirzaee, E., Sartaj, M. (2022). Activated carbon-based magnetic composite as an adsorbent for removal of polycyclic aromatic hydrocarbons from aqueous phase: Characterization, adsorption kinetics, and isotherm studies. *Journal of Hazardous Materials*. 6, 100083. DOI: 10.1016/j.hazadv.2022.100083.

- [33] Khumalo, S.M., Bakare, B.F., Rathilal, S. (2024). Single and multicomponent adsorption of amoxicillin, ciprofloxacin, and sulfamethoxazole on chitosancarbon nanotubes hydrogel beads from aqueous solutions: kinetics, isotherms, and thermodynamic parameters.

 Journal of Hazardous Materials. 13, 100404. DOI: 10.1016/j.hazadv.2024.100404.
- [34]Ji. W.H., Guo, Y.S., Wang, X., Lu, X.F., Guo, D.S. (2019). Amino-modified covalent organic framework as solid phase extraction absorbent for of determination carboxylic acid pesticides in environmental water samples. Journal of Chromatography A. 11-18.DOI: 10.1016/j.chroma.2019.02.048.
- [35] Hayat, W., Du, X., Liu, Z., Hussain, I., Naseem, K., Zhang, Y. (2024). Removal of methomyl in water by leavesgenerated biochar: Effect of metallic coating, kinetics, and important role of hydroxyl radical. Surfaces and Interfaces. 48, 104306. DOI: 10.1016/j.surfin.2024.104306.
- [36] Yu, Y., Liu, Ye., Hao, L., Zhu, B., Yang, Xi., Ge, S. (2024). Enhanced adsorption and cytotoxicity of hydrothermally aged microplastics for volatile organic compounds in sludge. *Journal of Environmental Chemical Engineering*. 12, 112104. DOI: 10.1016/j/jece.2024/112104.